Rheology of liquid fcc metals: Equilibrium and transient-time correlation-function nonequilibrium molecular dynamics simulations

Caroline Desgranges and Jerome Delhommelle
Department of Chemical Engineering, University of South Carolina, Columbia, South Carolina 29208, USA
and Department of Chemistry, University of North Dakota, Grand Forks, North Dakota 58202, USA
(Received 17 February 2008; revised manuscript received 15 August 2008; published 13 November 2008)

Using classical molecular dynamics simulation together with the quantum-corrected Sutton-Chen many-body embedded-atom model, we study the rheology of several liquid fcc metals (Pb, Pt, Ir, Ag, and Rh) at ambient pressure and at four temperatures ranging from 5% below the melting temperature to 75% above the melting temperature. We first carry out equilibrium molecular dynamics simulations and determine, using Green-Kubo's formalism, the shear viscosity η_{GK}, the shear modulus G_∞, and the Maxwell relaxation time τ_M. By scaling the shear stress autocorrelation function or, equivalently, the time-dependent viscosity $\eta(t)$ by η_{GK} and the time t by τ_M, we show that the scaled time-dependent viscosity for all metals collapses onto the same curve. This demonstrates that the relaxation behavior is the same for all metals studied here. We then apply transient-time correlation-function nonequilibrium molecular dynamics simulations to determine the response of liquid metals subjected to shear rates ranging from 10 s^{-1} to 5×10^{12} s^{-1}. We show that for all metals, the shear rate-dependent viscosity $\eta(\dot{\gamma})$ (scaled by η_{GK}) as a function of the applied shear rate $\dot{\gamma}$ (scaled by the inverse of τ_M) collapses onto the same curve. We obtain the same result for the shear rate-dependent pressure $P(\dot{\gamma})$ (scaled by G_∞) and for the potential energy (scaled by its equilibrium value). Fits to power-law expressions show that $\eta(\dot{\gamma})$ follows the prediction of mode-coupling theory and that nonanalytic exponents are found for the shear rate dependence of pressure and potential energy.

DOI: 10.1103/PhysRevB.78.184202 PACS number(s): 66.20.−d, 61.20.−p, 61.25.−f

I. INTRODUCTION

Transport properties, such as shear viscosity, play a central role in many applications ranging from biological systems to materials processing. An understanding of how the liquid responds when subjected to an external field is essential in analyzing the behavior of liquids and supercooled liquids. Computational physics methods, i.e., *ab initio* and classical molecular dynamics (MD) simulations, have proved to be a valuable tool in helping us understand how the structure and in turn the transport properties of liquids are affected by shear. Previous work based either on *ab initio*[1] or on classical molecular dynamics simulations[2,3] have demonstrated how the shear viscosity of liquid metals could be determined through the evaluation of the shear stress autocorrelation function and of Green-Kubo relations.[4] A complete understanding of the rheology of liquid metals using molecular simulations has remained elusive so far. Nonequilibrium molecular dynamics (NEMD) simulations should be, in principle, of great help since they provide a direct access to the microscopic structural changes induced by the applied shear rate. However, most NEMD studies have been restricted so far to liquid metals subjected to very high shear rates, i.e., several orders of magnitude higher than the experimentally accessible rates. For instance, in previous work,[2,3] the shear rates explored by NEMD simulations were at least of the order of 10^{10} s^{-1} and mostly one to two orders of magnitude higher. As a result, in these simulations, liquid metals exhibited a pseudoplastic fluid behavior and underwent shear thinning over the range of shear rates simulated. We showed in recent work[5] how the transient-time correlation-function (TTCF) formalism[6–9] could be applied to determine the rheology of a liquid metal during the course of nonequilibrium molecular dynamics (TTCF-NEMD) simulations. The transient-time correlation-function formalism is essentially a simple nonlinear generalization of the Green-Kubo relations. The TTCF-NEMD method is a marked improvement over conventional NEMD methods since TTCF-NEMD simulations allow the studying of the response of systems subjected to an arbitrarily low (i.e., realistic) shear rate.

The objective of this work is twofold. Our first goal is to assess the ability of the quantum-corrected Sutton-Chen embedded-atom model (qSC-EAM) (Refs. 10 and 11) potential to predict shear viscosities that are in good agreement with the experimental data for liquid Pb, Pt, Ir, Ag, and Rh. Having a simple and accurate model for liquid fcc metals, which can be used in classical molecular dynamics simulations, is essential for many applications. This is the case here since, as we will see, the TTCF-NEMD simulations we carry out to study the rheology of liquid Pb, Pt, Ir, Ag, and Rh requires simulation of the time evolution of the system over tens of thousands of molecular dynamics trajectories of ten picoseconds each (i.e., well beyond reach of *ab initio* molecular dynamics studies, which typically involve simulating a single trajectory over a few tens of picoseconds[1]). Having such models is also crucial in many other types of study such as, for instance, the simulations of crystallization from liquid metals,[12,13] which require simulating the time evolution of large systems and over long-time intervals (typically of the order of 10^4–10^5 atoms and of several nanoseconds[14–17]). The second aim of this work is to demonstrate that all the liquid metals studied in this work present the same rheology. More specifically, by appropriately scaling the results of EMD as well as of TTCF-NEMD simulations, we will show that, for all liquid metals studied in this work: (i) the shear stress relaxation behavior is the same and, (ii) when sub-

TABLE I. Parameters, melting temperature ($T_{m,\mathrm{qSC}}$) of the qSC-EAM potential, and experimental melting temperature ($T_{m,\mathrm{exp}}$) for Pb, Pt, Ir, Ag, and Rh.

	Pb	Pt	Ir	Ag	Rh
a (Å)	4.9495	3.916 30	3.834 40	4.069 10	3.798 40
ε (10^{-2} eV)	0.557 72	0.978 94	0.376 74	0.394 50	0.246 12
c	45.882	71.336	224.815	96.524	305.499
m	7	7	6	6	5
n	10	11	13	11	13
$T_{m,\mathrm{qSC}}$ (K)	575	1925	2740	1000	2125
$T_{m,\mathrm{exp}}$ (K)	601	2042	2683	1234	2239

jected to a shear rate, the response, in terms of shear viscosity, departure from the equilibrium pressure, and potential energy, is the same for all systems. We will also determine from the TTCF-NEMD simulations how shear viscosity, pressure, and energy depend on the applied shear rate and compare our results to the predictions of mode-coupling theory and to previous simulation work.

The paper is organized as follows. In Sec. II, we present the qSC-EAM used for liquid Pb, Pt, Ir, Ag, and Rh. We give an account of the EMD and TTCF-NEMD methods used to evaluate the shear stress as well as the viscosity of liquid Pb, Pt, Ir, Ag, and Rh. We then present and discuss the results obtained at ambient pressure and at four different temperatures, ranging from 5% below the melting point to 75% above the melting point.

II. QUANTUM-CORRECTED SUTTON-CHEN EMBEDDED-ATOM MODEL POTENTIAL

The accuracy of the classical MD simulations relies on the ability of the model used in these simulations to reproduce either experimental data or the results of *ab initio* calculations. A simple and accurate model is the embedded atom model (EAM) potential,[18] which can be derived by a second moment approximation to tight-binding molecular-orbital theory.[19] In this work, we use the qSC-EAM (Refs. 10 and 11) to model the interactions in liquid Pb, Pt, Ir, Ag, and Rh. For a system of N atoms, the potential energy U is written as the sum of a contribution arising from pairwise interactions and a contribution of a many-body term,

$$U = \frac{1}{2}\sum_{i=1}^{N}\sum_{j\neq i}\varepsilon\left(\frac{a}{r_{ij}}\right)^{n} - \varepsilon C\sum_{i=1}^{N}\sqrt{\rho_i}, \tag{1}$$

in which r_{ij} is the distance between two atoms i and j, and the density term ρ_i is given by

$$\rho_i = \sum_{j\neq i}\left(\frac{a}{r_{ij}}\right)^{m}. \tag{2}$$

We give in Table I the parameters used in this work. We also provide in Table I the melting temperatures of the qSC-EAM potential obtained from two-phase molecular simulations[11] together with the experimental data. The melting temperatures predicted by the qSC-EAM potential are generally in excellent agreement with the experimental data (within 5% for Pb, 6% for Pt, 3% for Ir, and 5% for Rh), with the exception of Ag for which the agreement is only good (within 19%).

III. SIMULATION METHODS

We first determine through a series of molecular dynamics simulations carried out at constant temperature and constant pressure, the equilibrium densities for all liquid metals considered at ambient pressure and temperatures: (i) 5% below the melting point, (ii) at the melting point, (iii) 10% above the melting point, and (iv) 75% above the melting point. Then, in order to determine the shear viscosity and study the rheology of liquid metals for each set of conditions, we carry out EMD and TTCF-NEMD simulations on systems of $N=256$ atoms in the NVT ensemble, in which the volume of

TABLE II. Rheology of liquid Pb at ambient pressure: simulated density ρ_{sim}, shear viscosity [η_{exp}: experimental data (Refs. 20 and 21) and η_{GK}: Green-Kubo estimates], infinite frequency shear modulus G_∞, and Maxwell relaxation time τ_M.

T (K)	ρ_{sim} (g cm^{-3})	η_{exp} (mPa s)	η_{GK} (mPa s)	G_∞ (GPa)	τ_M (fs)
550	9.84		2.8 ± 0.1	9.3 ± 0.1	301 ± 4
575	9.79		2.4 ± 0.1	9.2 ± 0.2	258 ± 3
650	9.60	2.27	1.98 ± 0.05	9.0 ± 0.1	221 ± 2
1000	8.76		1.00 ± 0.05	8.0 ± 0.1	125 ± 2

TABLE III. Rheology of liquid Pt at ambient pressure: experimental (ρ_{exp}) (Ref. 22) and simulated (ρ_{sim}) densities, shear viscosity [η_{exp}: experimental data (Ref. 22) and η_{GK}: Green-Kubo estimates], infinite frequency shear modulus G_∞, and Maxwell relaxation time τ_M.

T (K)	ρ_{exp} (g cm^{-3})	ρ_{sim} (g cm^{-3})	η_{exp} (mPa s)	η_{GK} (mPa s)	G_∞ (GPa)	τ_M (fs)
1830	19.43	18.55	6.65	7.8 ± 0.2	65.2 ± 0.5	120 ± 2
1925	19.33	18.44	5.66	7.2 ± 0.2	64.9 ± 0.4	111 ± 2
2125	19.13	18.08	4.22	5.6 ± 0.2	62.5 ± 0.4	90 ± 1
3375		16.16		2.8 ± 0.05	52.5 ± 0.2	53 ± 1

the system V is chosen so that the ratio N/V matches the equilibrium density previously determined for each temperature. The equilibrium densities used in the simulation, together with the available experimental densities, are given in Tables II–VI.

In EMD simulations, we use the following set of equations of motion

$$\dot{\mathbf{r}}_i = \frac{\mathbf{p}_i}{m_i},$$

$$\dot{\mathbf{p}}_i = \mathbf{F}_i - \alpha \mathbf{p}_i, \tag{3}$$

where m_i denotes the mass of atom i and $\mathbf{F}_i$ denotes the force on atom i resulting from the interaction potential. α is the thermostat multiplier,[9] which fixes the kinetic energy, and hence, according to the equipartition principle, the temperature is defined as $T_{kin} = \langle \sum_{i=1}^{N} m_i \mathbf{v}_i^2 \rangle / 3Nk_B$, where k_B is Boltzmann's constant. α is given by

$$\alpha = \frac{\sum_{i=1}^{N} \mathbf{p}_i \cdot \mathbf{F}_i / m_i}{\sum_{i=1}^{N} \mathbf{p}_i^2 / m_i}. \tag{4}$$

During the simulation run, the shear stress is evaluated as the opposite of $P_{xy} = \Sigma_i (p_{xi} p_{yi}/m + F_{xi} y_i)/V$. Shear viscosity is then estimated according to the following Green-Kubo expression:

$$\eta = \frac{V}{k_B T} \int_0^\infty \langle P_{xy}(s) P_{xy}(0) \rangle ds. \tag{5}$$

The TTCF-NEMD method consists of monitoring the response of a system over a large number of nonequilibrium trajectories. For that purpose, we generate many equilibrium configurations during the course of a long equilibrium trajectory [governed by Eq. (3)]. Each of these configurations is the starting point for a nonequilibrium trajectory. The nonequilibrium trajectory is generated by a homogeneous shear field in the SLLOD equations of motion[9] together with appropriate periodic boundary conditions.[24] This method correctly describes an isolated bulk system under arbitrarily strong shear.[9] For a fluid undergoing Couette flow in the x direction with a velocity gradient along the y direction, the SLLOD equations for a particle i are as follows:

$$\dot{\mathbf{r}}_i = \frac{\mathbf{p}_i}{m} + \dot{\gamma} y_i \mathbf{e}_x,$$

$$\dot{\mathbf{p}}_i = \mathbf{F}_i - \dot{\gamma} p_{y_i} \mathbf{e}_x - \alpha \mathbf{p}_i, \tag{6}$$

where $\dot{\gamma}$ is the imposed shear rate and $\mathbf{e}_x$ is a unit vector along the x axis. In this case, the thermostat multiplier α fixes the peculiar kinetic energy, i.e., the kinetic energy relative to the flow, and hence the temperature defined as

$$T_{kin} = \frac{\sum_i m_i (\mathbf{v}_i - \dot{\gamma} y_i \mathbf{e}_x)^2}{3Nk_B}, \tag{7}$$

α is given by

$$\alpha = \frac{\sum_i (\mathbf{F}_i \cdot \mathbf{p}_i - \dot{\gamma} p_{x_i} p_{y_i})}{\sum_i \mathbf{p}_i \cdot \mathbf{p}_i}. \tag{8}$$

The TTCF formalism may be used to determine the shear viscosity, and more generally any phase-space property, of fluids undergoing shear flow.[5,9] For any phase-space property $B(t)$, the average of B at time t is equal to

TABLE IV. Rheology of liquid Ir at ambient pressure: experimental (Ref. 23) (ρ_{exp}) and simulated (ρ_{sim}) density, shear viscosity [η_{exp}: experimental data (Ref. 23) and η_{GK}: Green-Kubo estimates], infinite frequency shear modulus G_∞, and Maxwell relaxation time τ_M.

T (K)	ρ_{exp} (g cm^{-3})	ρ_{sim} (g cm^{-3})	η_{exp} (mPa s)	η_{GK} (mPa s)	G_∞ (GPa)	τ_M (fs)
2600	19.6	19.15	7.41	10.7 ± 0.2	103 ± 1	104 ± 1
2740	19.48	18.44	6.91	10.0 ± 0.2	101 ± 1	99 ± 1
3000	19.22	18.08		7.7 ± 0.2	98 ± 1	79 ± 1
4800		16.16		3.0 ± 0.1	75 ± 1	40 ± 1

TABLE V. Rheology of liquid Ag at ambient pressure: simulated density ρ_{sim}, Green-Kubo estimates for the shear viscosity η_{GK}, infinite frequency shear modulus G_∞, and Maxwell relaxation time τ_M.

T (K)	ρ_{sim} (g cm^{-3})	η_{GK} (mPa s)	G_∞ (GPa)	τ_M (fs)
950	9.23	5.0 ± 0.2	29.9 ± 0.4	167 ± 2
1000	9.14	4.0 ± 0.1	29.3 ± 0.3	136 ± 2
1100	9.00	3.05 ± 0.05	28.4 ± 0.4	107 ± 2
1750	8.10	1.45 ± 0.05	23.9 ± 0.2	61 ± 1

$$\langle B(t)\rangle = \langle B(0)\rangle - \frac{V\dot{\gamma}}{k_B T}\int_0^t \langle B(s)P_{xy}(0)\rangle ds. \quad (9)$$

If we choose $B(t)=P_{xy}(t)$, the equilibrium average $\langle P_{xy}(0)\rangle$ is equal to zero and we obtain the following expression for $\langle P_{xy}(t)\rangle$:

$$\langle P_{xy}(t)\rangle = -\frac{V\dot{\gamma}}{k_B T}\int_0^t \langle P_{xy}(s)P_{xy}(0)\rangle ds. \quad (10)$$

It is then straightforward to evaluate the shear viscosity according to

$$\langle \eta(t)\rangle = \frac{V}{k_B T}\int_0^t \langle P_{xy}(s)P_{xy}(0)\rangle ds. \quad (11)$$

The TTCF approach is particularly advantageous over conventional NEMD methods since it allows studying of the response of the fluid for experimentally accessible shear rates[5,25–31] (it has also been applied in previous work to simple liquids undergoing elongational flow[32] and to determine the electric conductivity in molten sodium chloride[33]). An additional advantage is that a number of issues arising from the very large shear rates used in conventional NEMD methods will not affect the TTCF calculations such as, e.g., the effect of the thermostatting method on the results. In simulations, dissipation of heat is accounted for by a homogeneous thermostatting force which fixes the expression for the temperature given in Eq. (7) and enables the system to reach a steady state. When the applied shear rate is large,[34,35] the flow velocity is known to depart from the linear profile assumed in the expression for the temperature given in Eq. (7). In this case, using a thermostat based on Eq. (7) might result in an artificially low estimate for the viscosity at high shear rates.[36–38] This problem can be circumvented by using a configurational thermostat[39,40] based on a purely configurational expression of the temperature.[41–44] However, previous work on a variety of atomic[45,46] and molecular fluids[47,48] has shown that both types of thermostats give the same results (both for the energy and the viscosity) for shear rates below 10^{12} s^{-1}. Since the aim of this work is to determine the response of liquid fcc metals subjected to experimentally accessible shear rates, i.e., several orders of magnitudes smaller than 10^{12} s^{-1}, we will use the most computationally efficient strategy, i.e., the Gaussian thermostat presented in Eq. (6).

TABLE VI. Rheology of liquid Rh at ambient pressure: simulated density (ρ_{sim}), Green-Kubo estimates for the shear viscosity η_{GK}, infinite frequency shear modulus G_∞, and Maxwell relaxation time τ_M.

T (K)	ρ_{sim} (g cm^{-3})	η_{GK} (mPa s)	G_∞ (GPa)	τ_M (fs)
2125	10.64	8.0 ± 0.1	84 ± 1	96 ± 2
2340	10.44	5.7 ± 0.1	81 ± 1	70 ± 2
3720	9.27	2.4 ± 0.1	65 ± 1	38 ± 1

We integrate the equations of motion with the operator splitting algorithms proposed by Zhang[49] for the EMD simulations and Pan *et al.*[50] for the TTCF-NEMD simulations. In all cases, we use time steps of 5–10 fs. We also use a cut-off radius, set to be equal to twice the value of the parameter a, beyond which interactions between atoms are neglected. Periodic boundary conditions are applied to the system either in the standard form for EMD simulations[4] or in the form proposed by Lees and Edwards[24] for TTCF-NEMD simulations. For each liquid metal and each set of conditions, EMD simulations were run for 10 ns, over which the correlation function for the shear stress given in Eq. (5) was evaluated. The TTCF-NEMD simulations were carried out as follows. During a subsequent EMD simulation run, we selected 10 000 equilibrium configurations of the system at intervals of 10 ps. From each of these configurations, we defined three other equilibrium configurations: (i) by reversing the sign of the momenta of all particles (also termed as time-reversal mapping[9]), (ii) by mirror symmetry (reversing the sign of x and p_x for all particles), and (iii) by applying both the time-reversal mapping and the mirror symmetry. The 40 000 configurations so obtained were the starting points for the nonequilibrium trajectories. In addition to being more efficient, this procedure also ensures that the $\langle P_{xy}(0)\rangle$ is exactly zero.

IV. RESULTS AND DISCUSSION

We first present the results obtained from the EMD simulations. We report in Tables II–VI the densities, ρ_{sim}, obtained for the various state points for each liquid metal as well as the shear viscosities, η_{GK}, estimated according to the Green-Kubo relation given in Eq. (5), together with the available experimental data, ρ_{exp} and η_{exp}, respectively. For all metals considered here, the liquid densities predicted by the qSC-EAM are in very good agreement with the experimental data (within 5% for Pt and Ir, and within 2% for Rh for the state points considered). The ability of the qSC-EAM potential to predict the shear viscosity depends on the liquid metal as well as on the state point studied. The agreement is good, e.g., for Pb at $T=1.1T_m$ (η_{GK} underestimates η_{exp} by 12%) and for Pt at $T=0.95T_m$ (η_{GK} overestimates η_{exp} by 17%). As we increase the temperature, the departure of the value predicted by qSC-EAM from the experimental value increases. For instance, for Pt, at $T=0.95T_m$, the difference between the two is of 17%; at $T=T_m$, it is of 27% and at $T=1.1T_m$, it reaches 33%. On the other hand, the agreement

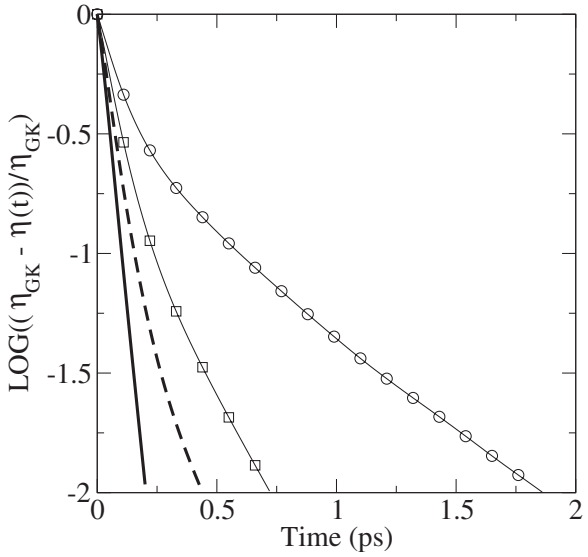

FIG. 1. Logarithm of $[\eta_{GK}-\eta(t)]/\eta_{GK}$ as a function of time at $T=1000$ K (solid line), $T=800$ K (dashed line), $T=650$ K (squares), and $T=550$ K (circles)].

between the shear viscosity predicted by the qSC-EAM and the experimental value is only fair for Ir. The qSC-EAM overestimates η_{exp} for the two lower temperatures by 41% and 44%, respectively. We recall that experimental data for the viscosity are only available at temperatures close to the experimental value for the melting temperature. Therefore, since the melting temperature predicted by qSC-EAM is higher than the experimental value (unlike for the other metals), it makes sense that qSC-EAM overestimates η_{exp} for these temperatures. It should also be noted that Sutton-Chen potentials are known to break down for solids where bond anisotropy becomes important (e.g., the adatom migration in Ir is not correctly predicted by the SC-EAM potential which ignores angle-dependent forces[51]). This could also play a role in the lesser ability of the qSC-EAM potential to predict the shear viscosity in the case of Ir.

We now compare the shear stress relaxation behavior observed for all systems. For this purpose, we start by applying the Maxwell model of viscoelasticity[52] to the liquid metals studied in this work. The Maxwell model has been shown to correctly describe a variety of systems, such as simple liquids[52] and molten salts.[46] The Maxwell model, in which the shear stress autocorrelation function (i.e., the memory function) is assumed to decay exponentially, provides a route toward the evaluation of a relaxation time τ_M for the system. In the Maxwell model, the characteristic decay time τ_M is calculated as $\tau_M=\eta/G_\infty$, where $G_\infty=V\langle P_{xy}^2(0)\rangle/k_BT$ is the infinite frequency shear modulus. The calculated values for G_∞ and τ_M are given in Tables II–VI. We also plot in Fig. 1 the variation with time of the logarithm of $[\eta_{GK}-\eta(t)]/\eta_{GK}$ in the case of Pb for the four state points studied (this should appear as a line if the system is correctly described by the Maxwell model). As shown in Fig. 1, liquid Pb rigorously follows the Maxwell model for temperatures well above the melting temperature ($T=1000$ K, i.e., 75% above the melting temperature of the model). However, for temperatures below $T=1000$ K, the values of τ_M are much shorter than the time needed for $\eta(t)$ to reach its plateau (see Fig. 1). In fact, Fig. 1 shows that liquid Pb obeys the Maxwell model for very short times only. For instance, for $T=550$ K and for times below 0.5 ps, we find the slope of the logarithm of $[\eta_{GK}-\eta(t)]/\eta_{GK}$ to be in excellent agreement with the value of the Maxwell relaxation time. Similar results are observed for the other metals.

We then scale the time-dependent viscosity $\eta(t)$ defined by

$$\eta(t)=\frac{V}{k_BT}\int_0^t\langle P_{xy}(s)P_{xy}(0)\rangle ds, \tag{12}$$

and the time t by η_{GK} and τ_M, respectively, for each liquid metal and for each state point considered in this work. For each state point, we collapse on the same graph the plots obtained for all liquid metals of the scaled time-dependent viscosity against the scaled time (Fig. 2). The main conclusion we draw from Fig. 2 is the fact that there is an excellent agreement between the results obtained for all liquid metals at the same state point. This convincingly demonstrates that the shear stress relaxation behavior is the same for all the liquid metals for a given state point. However, although the relaxation behavior is the same for all metals, it is state point dependent. As temperature decreases, it takes a longer time (even scaled by τ_M) for the ratio $\eta(t)/\eta_{GK}$ to reach its limiting value of one. For instance, this ratio reaches one within the first $5\times\tau_M$ for $T=1.75T_m$ and approximately $20\times\tau_M$ for $T=0.95T_M$.

We now turn to the results obtained for the rheology of liquid metals obtained during the TTCF-NEMD simulations. We start by showing in Fig. 3 the results obtained for the rheology of liquid Pb at $T=550$ K ($T=0.95T_m$). This three-dimensional plot, representing the variations of shear viscosity as a function of time and of the logarithm of the shear rate, provides a full picture of the rheology of liquid Pb. The region associated with short times represents the transient regime. The plateau region associated with large times and low enough shear rates represents the Newtonian regime. This finding is in agreement with recent experimental results showing that Pb melt behaves as a Newtonian liquid.[53] As shown in Fig. 3, the Newtonian plateau is reached for times larger than 4 ps and for shear rates lower than 10^7 s^{-1} (we emphasize again that this range of shear rates is not accessible by conventional NEMD methods). As the applied shear rate increases beyond 10^7 s^{-1}, the value of the shear viscosity in the steady state steadily decreases. In this region, liquid Pb enters the non-Newtonian regime and undergoes shear thinning.

As we did with the EMD results, we now compare the results obtained for the shear viscosity, pressure, and potential energy as a function of the applied shear rate for the various liquid metals studied here. The work carried out here brings two types of information on this issue. First, while many studies have focused on determining the shear rate dependence of these properties for systems modeled with pair potentials,[9] only a few studies have studied this issue with two- and three-body potentials[54,55] and none with many-body potentials such as the qSC-EAM potential used here.

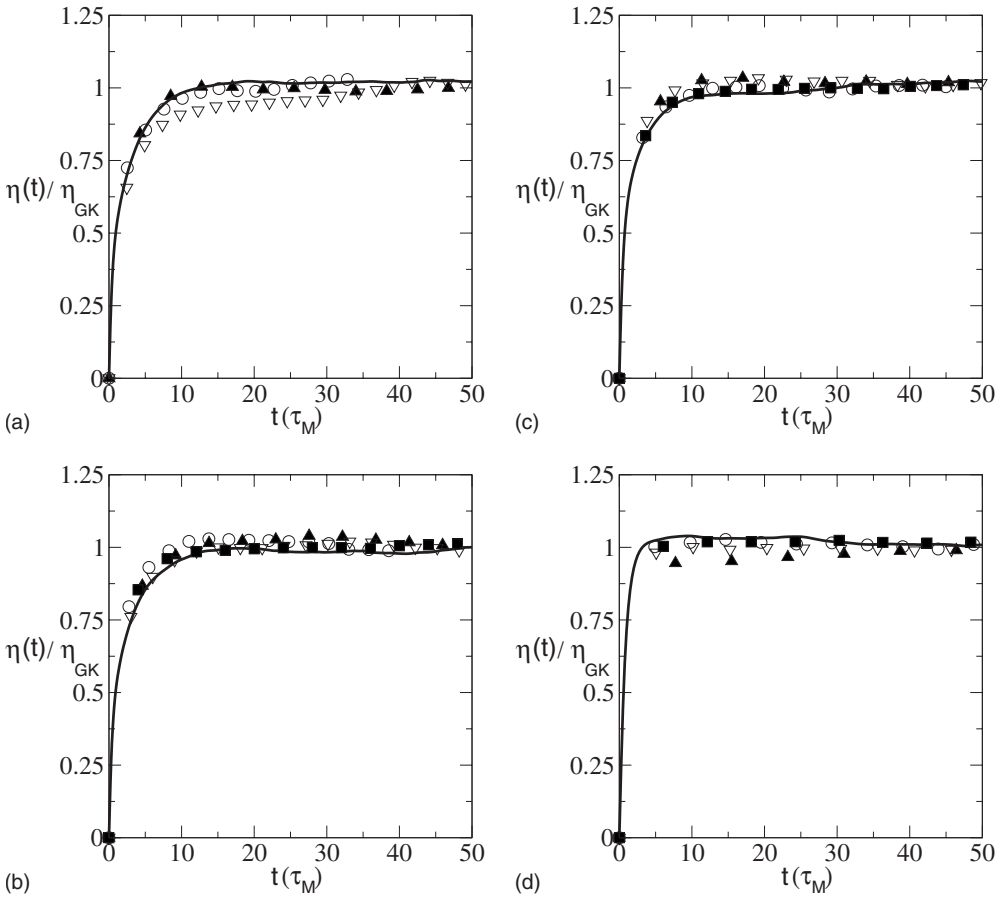

FIG. 2. $\eta(t)/\eta_{GK}$ as a function of t/τ_M for Pb (open circles), Pt (filled triangles up), Ir (solid line), Ag (open triangles down), and Rh (filled squares): (a) for a temperature 5% below the respective melting points, (b) at their respective melting point, (c) for a temperature 10% above their respective melting points, and (d) for a temperature 75% above their respective melting points.

Second, previous NEMD have focused on the very high shear rate regime, which makes it difficult to relate the simulation results to the predictions of the mode-coupling theory (valid in the limit of zero shear rate).[56] On the other hand, a connection between the predictions of the mode-coupling theory and the TTCF-NEMD results obtained here can be made since the TTCF-NEMD method allows the study of the response of liquid metals subjected to an arbitrarily low shear rate.

We first consider the dependence of shear viscosity on the applied shear rate. We start by scaling the viscosity $\eta(\dot{\gamma})$ obtained for an applied shear rate $\dot{\gamma}$ by η_{GK} and by scaling $\dot{\gamma}$ by the inverse of τ_M. We then collapse the results obtained for all liquid metals in Fig. 4 for $T=T_m$ and fit the results by the following expression:

$$\eta(\dot{\gamma})/\eta_{GK} = 1 - A(\dot{\gamma}\tau_M)^{\beta}, \tag{13}$$

where A and β are two fitting parameters. Fitting the simulation results for each metal leads to the following range for the two fitting parameters: $1.05 < A < 1.28$ and $0.45 < \beta < 0.59$. If we now include in the fitting procedure the simulation results obtained for all metals, we obtain $A=1.136$ and $\beta=0.504$ with a root-mean-square (rms) deviation of 0.045. The value of the exponent β is in excellent agreement with the prediction of the mode-coupling theory ($\beta=0.5$). We therefore conclude that the shear rate dependence of viscosity of liquid metals is that predicted by mode-coupling theory (we also plot in Fig. 4 the fit to the prediction of the mode-coupling theory, i.e., β fixed at 0.5 and $A=1.127$, with a rms deviation of 0.045).

We now move on to the shear rate dependence of the different contributions to the potential energy. We scale the two-body repulsive potential energy $U_{rep}(\dot{\gamma})$, the many-body attractive potential energy $U_{EAM}(\dot{\gamma})$, and the sum of these two contributions $U_{tot}(\dot{\gamma})$ by their equilibrium values. We

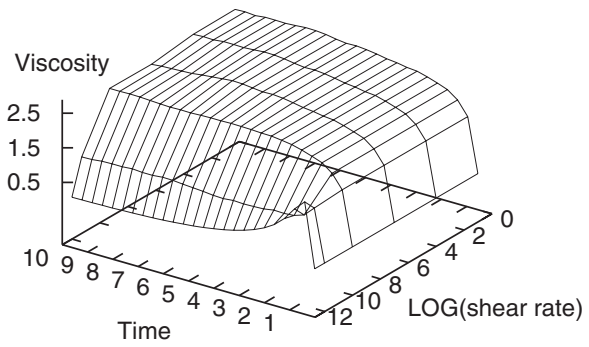

FIG. 3. Shear viscosity (in centipoise) as a function of time (in femtosecond) and of the logarithm of the shear rate (in s^{-1}) for Pb at $T=550$ K.

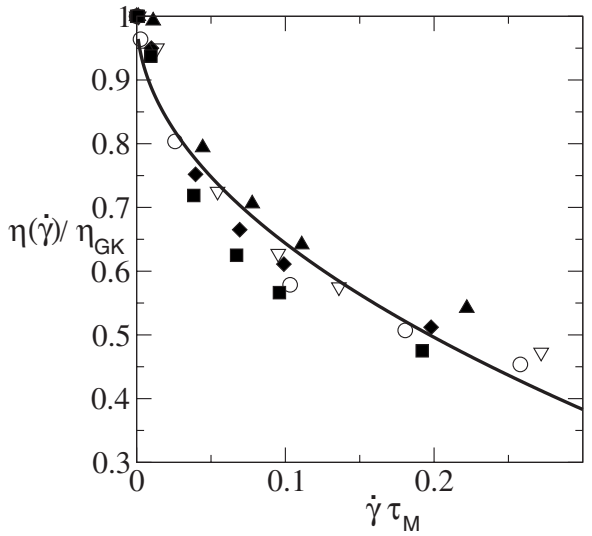

FIG. 4. $\eta(\dot{\gamma})/\eta_{\mathrm{GK}}$ as a function of $\dot{\gamma}\tau_M$ for Pb (open circles), Pt (filled triangles up), Ir (filled diamonds), Ag (open triangles down), and Rh (filled squares). The fit to the prediction of the mode-coupling theory is plotted as a solid line.

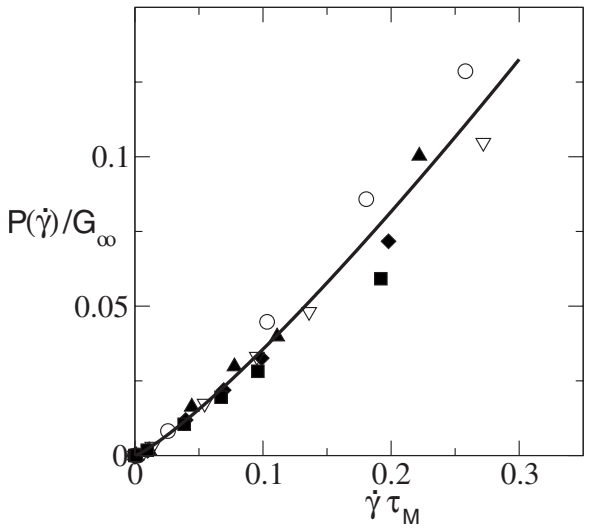

FIG. 6. Ratio of pressure $P(\dot{\gamma})$ in the sheared liquid metal over the shear modulus G_∞ as a function of $\dot{\gamma}\tau_M$: Pb (open circles), Pt (filled triangles up), Ir (filled diamonds), Ag (open triangles down), and Rh (filled squares). The fit to a power law is plotted as a solid line.

then collapse on the same graph the plots of these three quantities against the scaled shear rate $\dot{\gamma}$ (scaled again by the inverse of τ_M) for all metals in Fig. 5 and fit the results by the following expression:

$$U(\dot{\gamma})/U_{\mathrm{eq}} = 1 + A(\dot{\gamma}\tau_M)^{\beta}, \tag{14}$$

where A and β are two fitting parameters. Fitting the simulation results obtained for all metals leads to $A=0.445$ and $\beta=1.033$ with a rms deviation of 0.007 for the two-body contribution, to $A=0.095$ and $\beta=1.201$ with a rms deviation of 0.077 for the many-body contribution, and to $A=-0.089$ and $\beta=1.095$ with a rms deviation of 0.001 for the total potential energy. This last result shows that the shear rate dependence of the total potential energy follows neither the prediction of the mode-coupling theory, which suggests a value of β of 1.5, nor the analytic dependence observed in system modeled with two-body and Axilrod-Teller three-body interactions,[55] which suggested a value of β of 2.

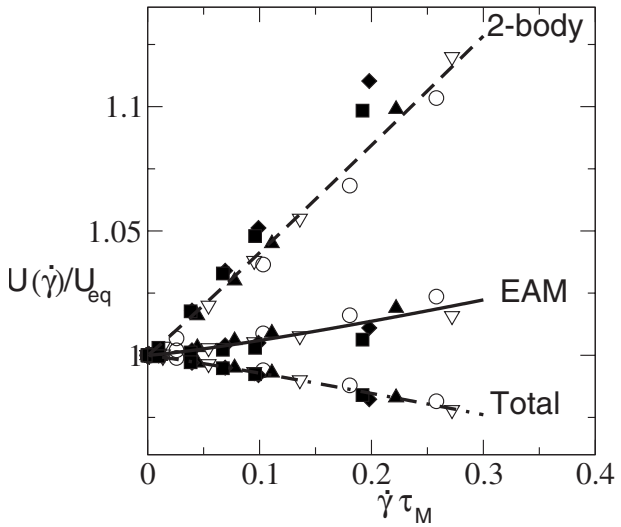

FIG. 5. Ratio of the potential energy $U(\dot{\gamma})$ in the sheared liquid metal over its equilibrium value U_{eq} as a function of $\dot{\gamma}\tau_M$. Top: repulsive two-body potential energy; middle: many-body EAM potential energy, and bottom: total potential energy. Pb (open circles), Pt (filled triangles up), Ir (filled diamonds), Ag (open triangles down), and Rh (filled squares). Fits to Eq. (14) are plotted as a dashed line (two-body potential energy), a solid line (EAM potential energy), and a dotted-dashed line (total potential energy).

We finally analyze the shear rate dependence of pressure. We scale the increase in hydrostatic pressure $P(\dot{\gamma})$ from its equilibrium value by the shear modulus G_∞. We then collapse on the same graph the plots of $P(\dot{\gamma})$ against the scaled shear rate $\dot{\gamma}\tau_M$ for all metals in Fig. 6 and fit the results by the following expression:

$$P(\dot{\gamma})/G_\infty = A(\dot{\gamma}\tau_M)^{\beta}, \tag{15}$$

where A and β are two fitting parameters. Fitting the simulation results obtained for all metals leads to $A=0.560$ and $\beta=1.197$ with a rms deviation of 0.006. This result shows again that the shear rate dependence of the total potential energy follows neither the prediction of the mode-coupling theory nor the analytic dependence observed in the system modeled with two-body and Axilrod-Teller three-body interactions.[55]

V. CONCLUSIONS

Using EMD simulations, we assess the ability of the qSC-EAM potential to predict the shear viscosity of liquid fcc metals at ambient pressure and at temperatures ranging from 5% below the melting temperature to 75% above the melting temperature. We show that while the model generally gives results that are in good agreement with the experimental data, some discrepancies are observed, e.g., in the case of Ir.

These discrepancies could be attributed to a too high melting temperature predicted by the model but could also be attributed to the fact that the model neglects angle-dependent forces. By appropriately rescaling the memory function or, equivalently, the time-dependent viscosity and the time, we demonstrate that the shear stress relaxation behavior is the same for all liquid metals studied in this work. We then extend these findings to nonequilibrium systems, when the liquid metal is subjected to a shear rate according to the TTCF-NEMD method. In particular, by appropriately rescaling the viscosity, pressure, and potential energy of the liquid metal under shear, we show that the shear rate dependence of all these quantities is the same for all metals considered here. We found the shear rate dependence of the shear viscosity following that predicted by the mode-coupling theory while, in contrast with the previous work on fluids modeled by potentials including a three-body contribution, we found nonanalytic exponents for the shear rate dependence of pressure and potential energy. More work needs to be done however to fully determine the dependence of the exponents of the shear rate for energy, pressure, and viscosity on the state point studied. As shown by Todd on the Lennard-Jones fluid, the exponents exhibited a strong dependence on density, and to a lesser extent on temperature, and the predictions of the mode-coupling theory were only adhered in the vicinity of the Lennard-Jones triple point. Todd[57] was also able to show that the exponents of the strain rate for energy, pressure, and viscosity were all linear functions of temperature and density. It remains to be seen whether such relations hold for many-body potentials such as the EAM potential used in this work to model liquid metals.

ACKNOWLEDGMENTS

Acknowledgment is given to the Donors of the American Chemical Society Petroleum Research Fund for partial support of this research.

[1] D. Alfe, G. Kresse, and M. J. Gillan, Phys. Rev. B **61**, 132 (2000).
[2] C. Desgranges and J. Delhommelle, Phys. Rev. B **76**, 172102 (2007).
[3] P. Xu, T. Cagin, and W. A. Goddard, J. Chem. Phys. **123**, 104506 (2005).
[4] M. P. Allen and D. J. Tildesley, *Computer Simulation of Liquids* (Clarendon, Oxford, 1987).
[5] C. Desgranges and J. Delhommelle, J. Chem. Phys. **128**, 084506 (2008).
[6] W. M. Visscher, Phys. Rev. A **10**, 2461 (1974).
[7] J. W. Dufty and M. J. Lidenfeld, J. Stat. Phys. **20**, 259 (1979).
[8] E. G. D. Cohen, Physica A **118**, 17 (1983).
[9] D. J. Evans and G. P. Morriss, *Statistical Mechanics of Nonequilibrium Liquids* (Academic, London, 1990).
[10] A. P. Sutton and S. Chen, Philos. Mag. Lett. **61**, 139 (1990).
[11] S. N. Luo, T. J. Ahrens, T. Cagin, A. Strachan, W. A. Goddard, and D. C. Swift, Phys. Rev. B **68**, 134206 (2003).
[12] C. Desgranges and J. Delhommelle, J. Am. Chem. Soc. **129**, 7012 (2007).
[13] C. Desgranges and J. Delhommelle, J. Chem. Phys. **127**, 144509 (2007).
[14] C. Desgranges and J. Delhommelle, Phys. Rev. Lett. **98**, 235502 (2007).
[15] C. Desgranges and J. Delhommelle, J. Am. Chem. Soc. **128**, 15104 (2006).
[16] C. Desgranges and J. Delhommelle, J. Am. Chem. Soc. **128**, 10368 (2006).
[17] J.-M. Leyssale, J. Delhommelle, and C. Millot, J. Am. Chem. Soc. **126**, 12286 (2004).
[18] M. S. Daw and M. I. Baskes, Phys. Rev. Lett. **50**, 1285 (1983).
[19] J. G. Ackland, M. W. Finnis, and V. Vitek, J. Phys. F: Met. Phys. **18**, L153 (1988).
[20] H. R. Thresh and A. F. Crawley, Metall. Trans. **1**, 1531 (1970).
[21] H. Jixin, G. Hongxuan, S. Jianjun, T. Xuelei, Z. Chengwei, Q. Xubo, and C. Xichen, Phys. Lett. A **358**, 171 (2006).
[22] T. Ishikawa, P. F. Paradis, and N. Koike, Jpn. J. Appl. Phys., Part 1 **45**, 1719 (2006).
[23] T. Ishikawa, P. F. Paradis, R. Fujii, Y. Saita, and S. Yoda, Int. J. Thermophys. **26**, 893 (2005).
[24] A. W. Lees and S. F. Edwards, J. Phys. C **5**, 1921 (1972).
[25] G. P. Morriss and D. J. Evans, Phys. Rev. A **39**, 6335 (1989).
[26] I. Borzsak, P. T. Cummings, and D. J. Evans, Mol. Phys. **100**, 2735 (2002).
[27] J. Petravic and P. Harrowell, Phys. Rev. E **71**, 061201 (2005).
[28] J. Delhommelle and P. T. Cummings, Phys. Rev. B **72**, 172201 (2005).
[29] G. Pan and C. McCabe, J. Chem. Phys. **125**, 194527 (2006).
[30] C. Desgranges and J. Delhommelle, Phys. Rev. E **77**, 027701 (2008).
[31] C. Desgranges and J. Delhommelle, Mol. Simul. **34**, 177 (2008).
[32] B. D. Todd, Phys. Rev. E **56**, 6723 (1997).
[33] J. Delhommelle, P. T. Cummings, and J. Petravic, J. Chem. Phys. **123**, 114505 (2005).
[34] J. Delhommelle, J. Petravic, and D. J. Evans, Phys. Rev. E **68**, 031201 (2003).
[35] J. Delhommelle, J. Petravic, and D. J. Evans, J. Chem. Phys. **119**, 11005 (2003).
[36] J. Delhommelle, Phys. Rev. E **71**, 016705 (2005).
[37] J. Delhommelle, Phys. Rev. B **69**, 144117 (2004).
[38] J. Delhommelle, J. Petravic, and D. J. Evans, J. Chem. Phys. **120**, 6117 (2004).
[39] J. Delhommelle and D. J. Evans, J. Chem. Phys. **115**, 43 (2001).
[40] L. Lue, O. G. Jepps, J. Delhommelle, and D. J. Evans, Mol. Phys. **100**, 2387 (2002).
[41] H. H. Rugh, Phys. Rev. Lett. **78**, 772 (1997).
[42] O. G. Jepps, G. Ayton, and D. J. Evans, Phys. Rev. E **62**, 4757 (2000).
[43] J. Delhommelle and D. J. Evans, J. Chem. Phys. **114**, 6229 (2001).
[44] J. Delhommelle and D. J. Evans, J. Chem. Phys. **114**, 6236 (2001).

[45] J. Delhommelle, Eur. Phys. J. E **15**, 65 (2004).
[46] J. Delhommelle and J. Petravic, J. Chem. Phys. **118**, 2783 (2003).
[47] J. Delhommelle and D. J. Evans, Mol. Phys. **99**, 1825 (2001).
[48] J. Delhommelle and D. J. Evans, J. Chem. Phys. **117**, 6016 (2002).
[49] F. Zhang, J. Chem. Phys. **106**, 6102 (1997).
[50] G. Pan, J. F. Ely, C. McCabe, and D. J. Isbister, J. Chem. Phys. **122**, 094114 (2005).
[51] R. M. Lynden-Bell, Surf. Sci. **259**, 129 (1991).
[52] J.-P. Hansen and I. R. McDonald, *Theory of Simple Liquids*, 3rd ed. (Academic, London, 2005).
[53] C. Sun, H. Geng, L. Ji, Y. Wang and G. Wang, J. Appl. Phys. **102**, 034901 (2007).
[54] S. H. Lee and P. T. Cummings, J. Chem. Phys. **101**, 6206 (1994).
[55] G. Marcelli, B. D. Todd, and R. J. Sadus, Phys. Rev. E **63**, 021204 (2001).
[56] K. Kawasaki and J. D. Gunton, Phys. Rev. A **8**, 2048 (1973).
[57] B. D. Todd, Phys. Rev. E **72**, 041204 (2005).